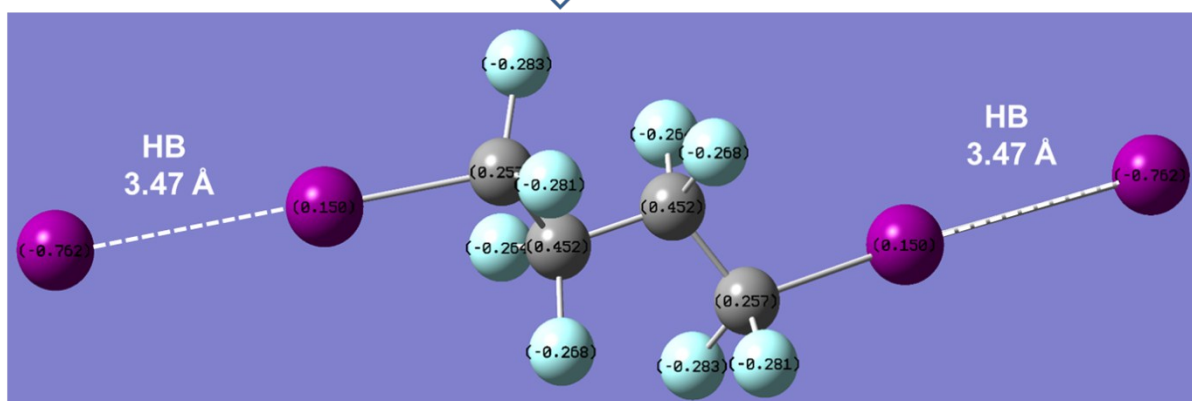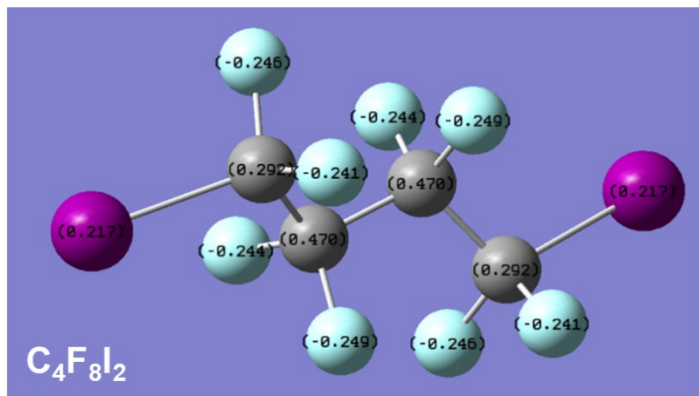# Supplementary Information

## Halogen Bonding Reduces Intrinsic Traps and Enhances Charge Mobilities in Halide Perovskite Solar Cells

*Shiqing Bi, Hui Wang, Jiyu Zhou, Shuai You, Yuan Zhang\*, Xinghua Shi, Huiqiong Zhou\*, and Zhiyong Tang*

a)

(-0.246)

(-0.244)  (-0.249)

(0.292)(-0.241)  (0.470)

(0.217)                                    (0.217)

(-0.244)(0.470)

(-0.249)     (-0.246)     (-0.241)

C₄F₈I₂

I⁻

(-0.283)

HB
3.47 Å                                    HB
                                          3.47 Å

(-0.26)(-0.268)

(0.25)                                    (-0.762)

(-0.281)

(0.150)

(-0.264)(0.452)  (0.452)

(0.150)

(-0.762)

(0.257)

(-0.268)     (-0.283)(-0.281)

b)

(0.214)          (0.246)

(0.214)          (0.246)

(0.080)  (-0.375)         (-0.627)

(-0.627)         (-0.375)                (0.080)

(0.246)          (0.214)

(0.246)          (0.214)

C₄H₈I₂

I⁻

(0.202)(0.202)

(-0.639)          (0.189)(0.189)

HB                                        (-0.351)                (-0.868)
3.74 Å

(0.084)          (-0.361)

(0.084)                   HB
                          3.74 Å

(-0.868)
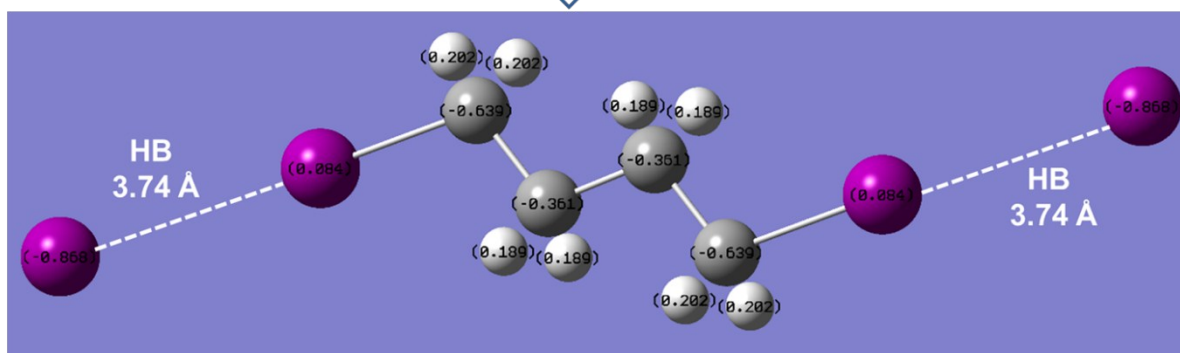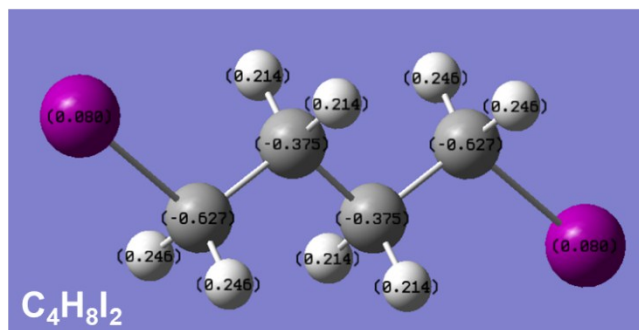
(0.189)(0.189)

(-0.639)

(0.202)(0.202)

S2

**Figure S1.** 3D chemical structures and halogen bonds with iodine anions illustrated by DFT calculations for (a) $C_4F_8I_2$ and (b) $C_4H_8I_2$ additives (purple: iodine, light blue: fluorene, grey: carbon, light grey: hydrogen). Dashed lines indicate the halogen bonds (HB) formed between the end group iodines with iodine anions in perovskite precursor solutions. Also included are the calculated Mulliken charges for iodines inside the additive molecules and the HB lengths.
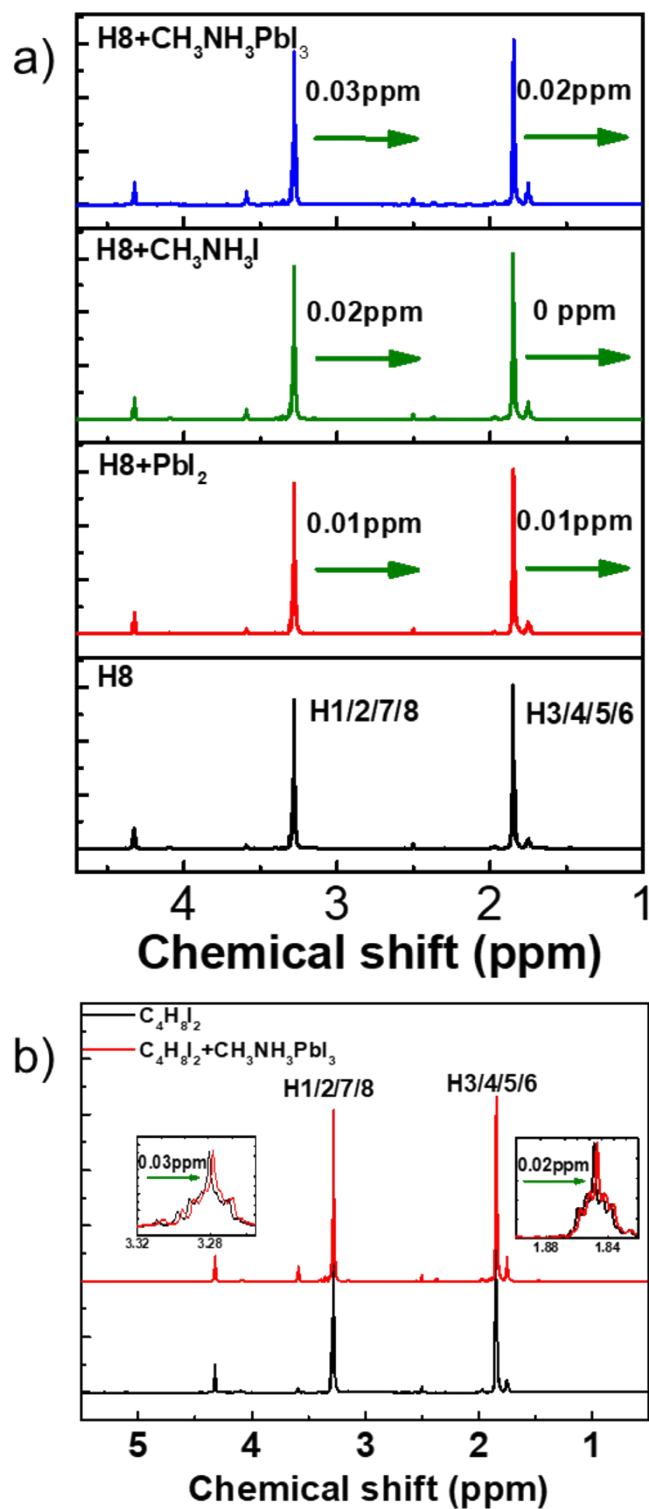
**Figure S2.** ^{1}H NMR spectra for pristine $C_4H_8I_2$ and $C_4H_8I_2$-added solutions of $PbI_2$, $CH_3NH_3I$, and $PbI_2$/$CH_3NH_3I$ mixtured. Insets in (b): zoommed-in spsctra at 3.28 and 1.85 ppm.
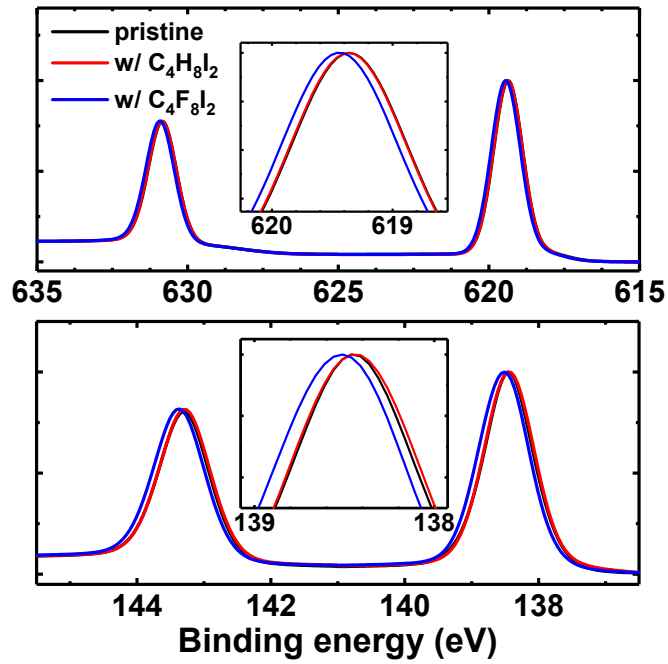
**Figure S3.** High-resolution X-ray photoelectron spectroscopy (XPS) of core level I 3d (upper panel) and Pb 4f (lower panel) measured on as-cast $CH_3NH_3PbI_3$ films. Inset: Zoomed-in spectra (normalized) of the 5/2 (I 3d) and 7/2 (Pb 4f) sub peaks to illustrate the upward shift of binding energy with additives.
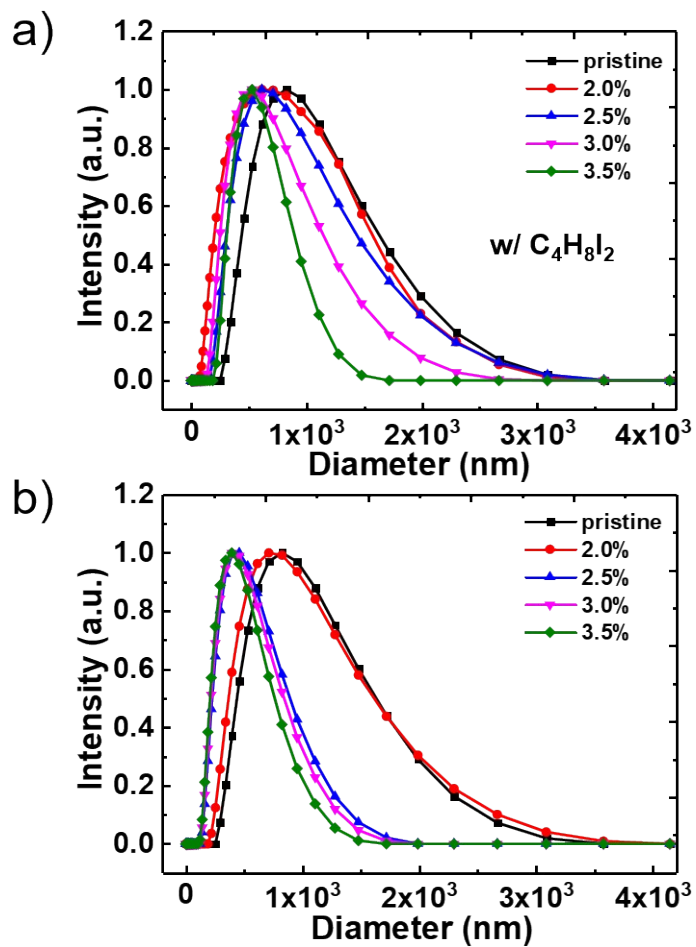
**Figure S4.** Diameter distribution for clusters in $CH_3NH_3PbI_3$ precursor solutions with various concentrations of (a) $C_4H_8I_2$ and (b) $C_4F_8I_2$ additives determined by dynamic light scattering.
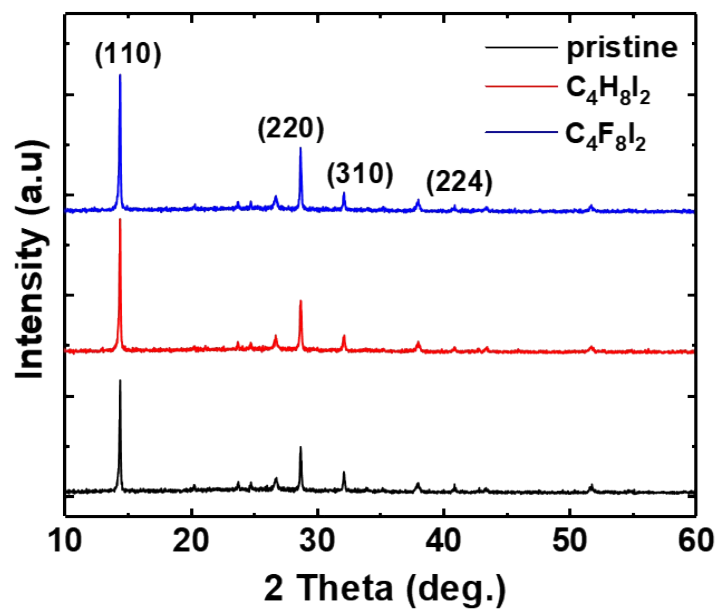
**Figure S5.** XRD patterns of annealed perovskite films prepared with different processing conditions.
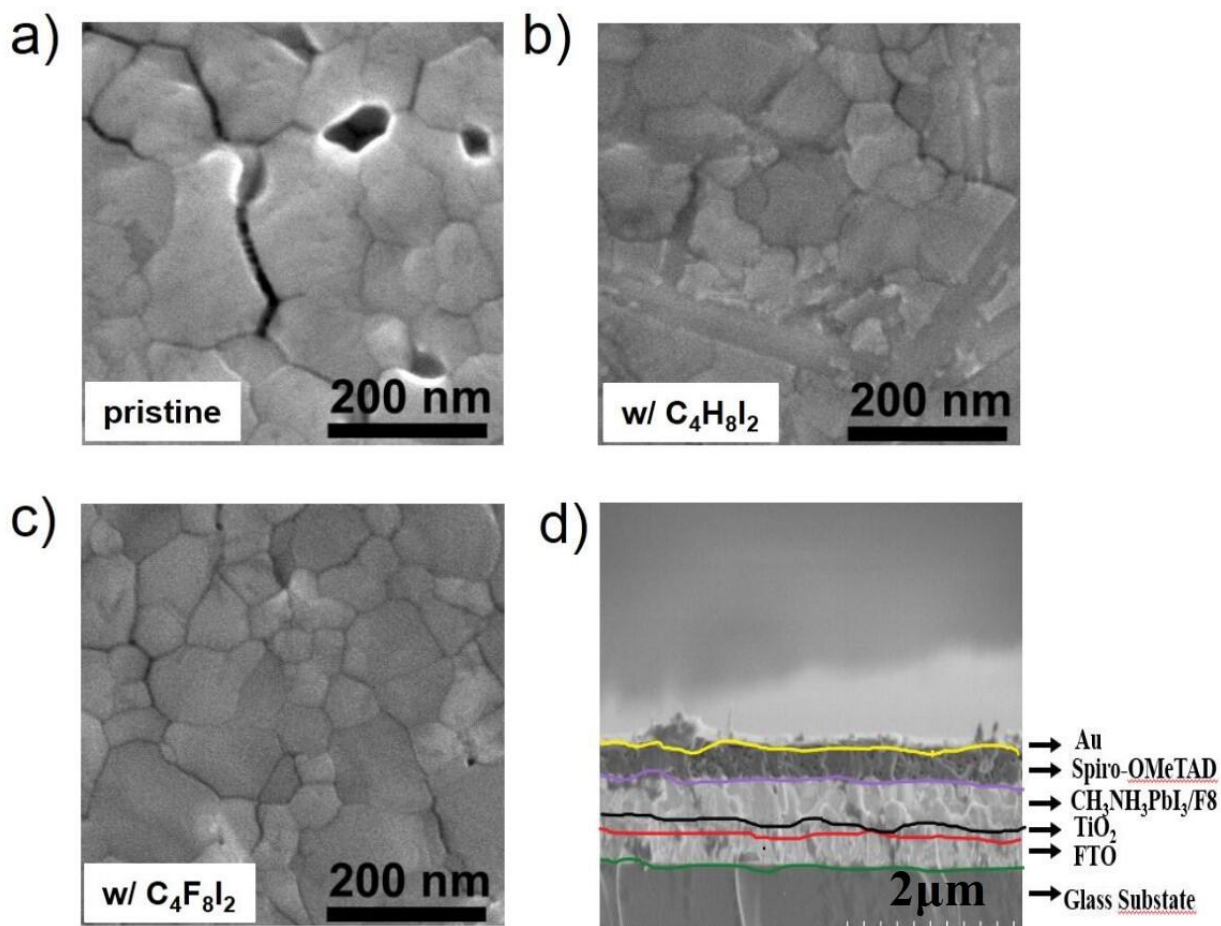
**Figure S6.** (a-c) Top-view scanning electron microscopic (SEM) images of as-spun films of CH$_3$NH$_3$PbI$_3$ without (a) and with C$_4$H$_8$I$_2$ (b) and C$_4$F$_8$I$_2$ (c) additives, (d) SEM cross section of our solar cell stucture.
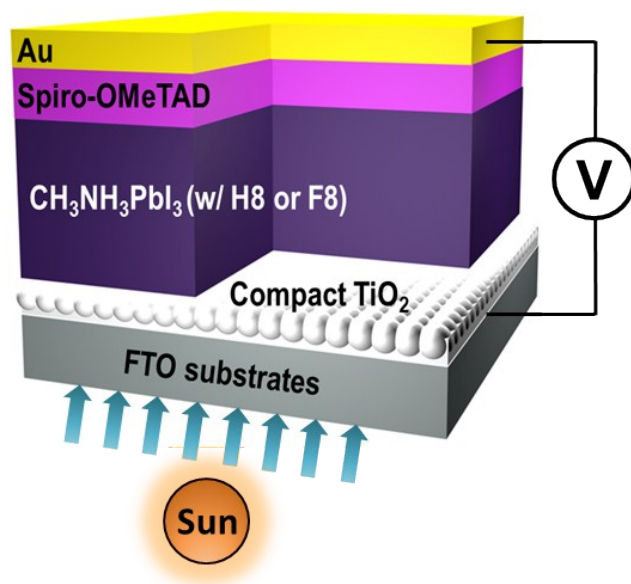
**Figure S7.** Sketched planar device architecture of $CH_3NH_3PbI_3$ solar cells based on FTO/compact $TiO_2$ cathode.
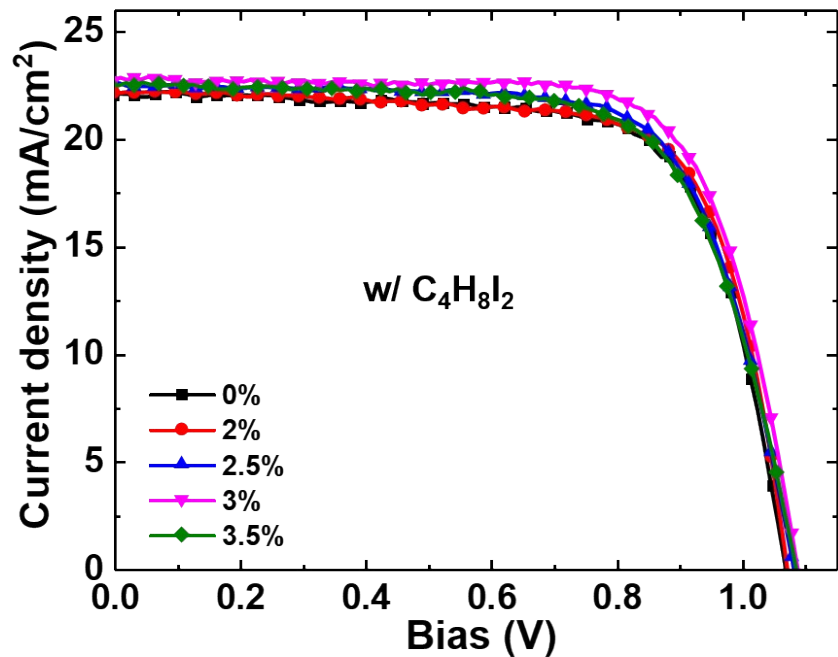
**Figure S8.** Current density versus voltage (*J-V*) characteristics of $CH_3NH_3PbI_3$ solar cells processed with different concentrations of $C_4H_8I_2$ additives (vol. ratio) in the reverse scan direction.
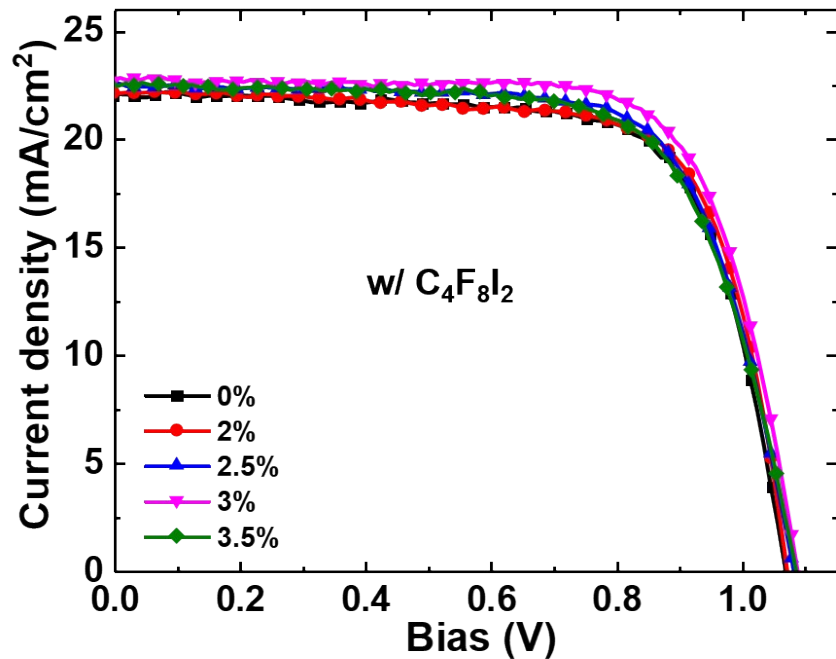
**Figure S9.** *J-V* characteristics of $CH_3NH_3PbI_3$ solar cells processed with various concentrations of $C_4F_8I_2$ additives in the reverse scan.
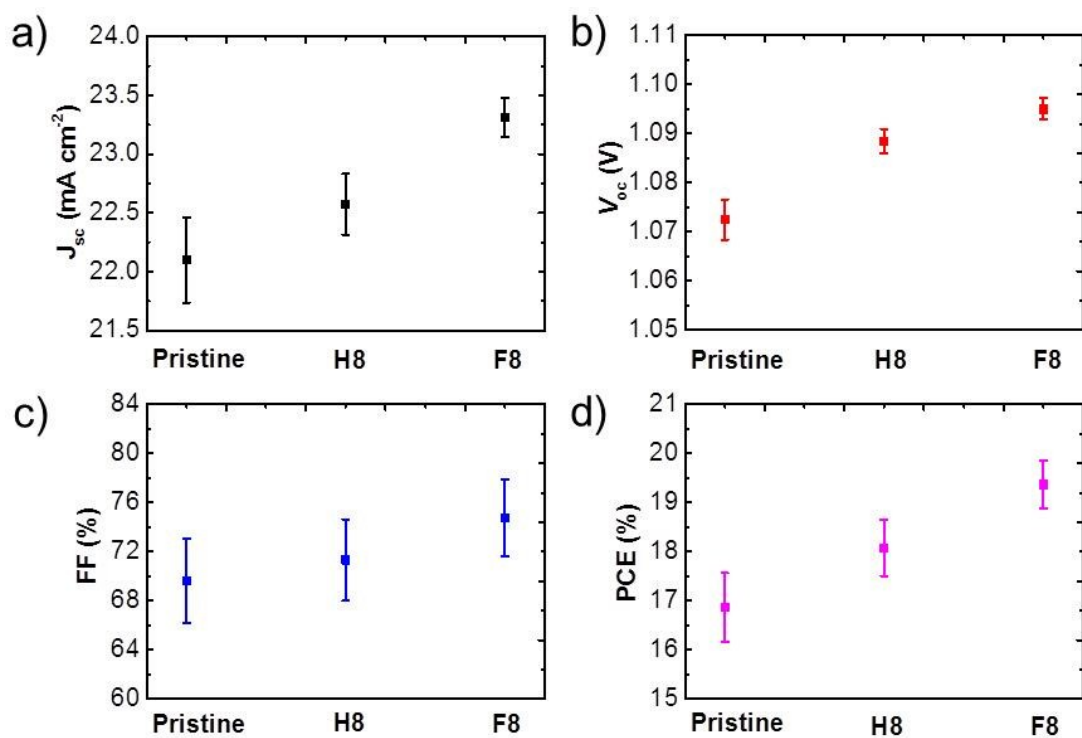
**Figure S10.** Averaged (a) $J_{sc}$, (b) $V_{oc}$, (c) FF, and (d) PCE of $CH_3NH_3PbI_3$ solar cells based on 20 devices in each condition. Also included are the statistical deviations of respective device parameters.
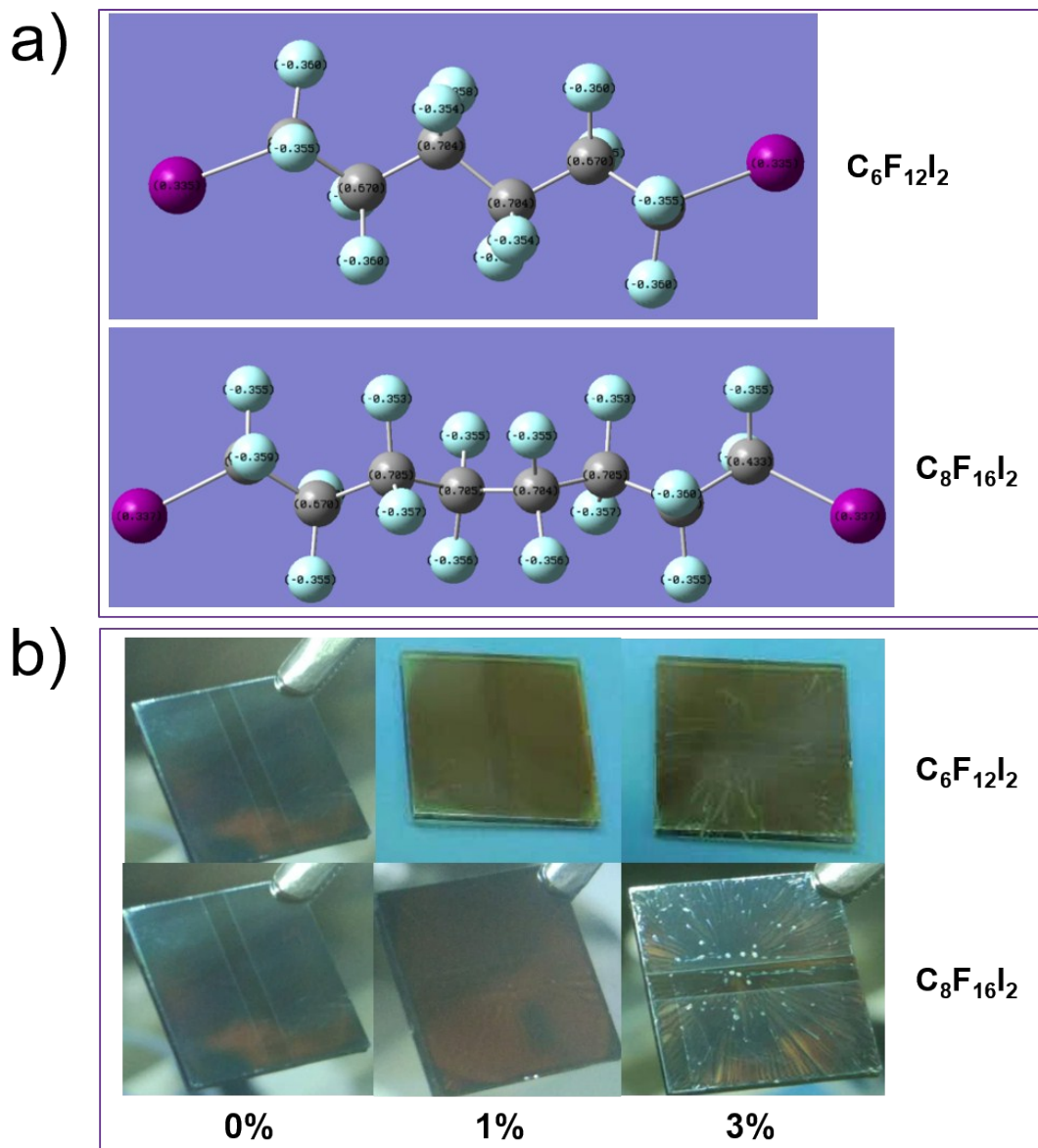
**Figure S11.** (a) Chemical structure of diiodoperfluoroalkyl additives of $C_6F_{12}I_2$ and $C_8F_{16}I_2$ with longer carbon chains obtained by DFT calculations together with the Mulliken charges for individual atoms. (b) Photos of the cast $CH_3NH_3PbI_3$ films processed with various concentrations of long-chain additives.
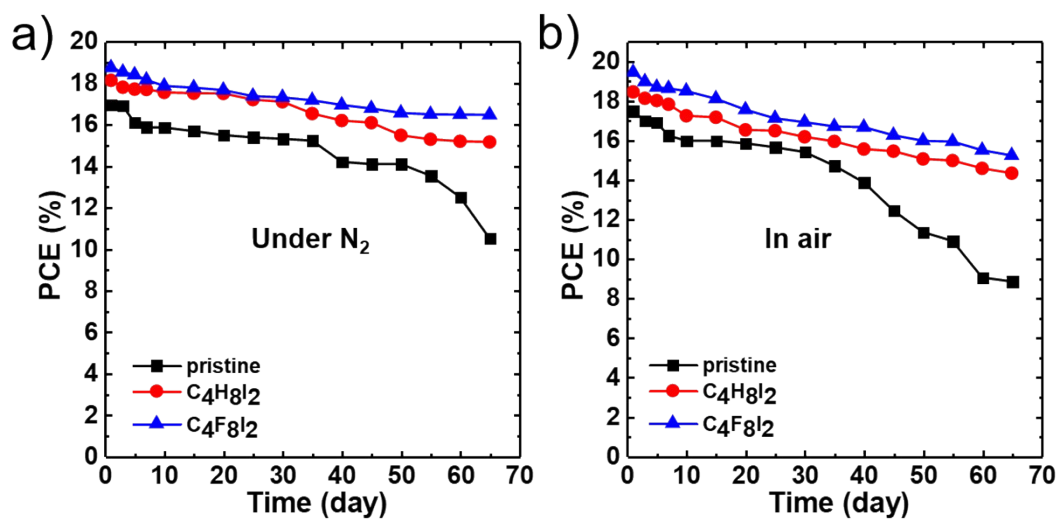
**Figure S12.** PCEs of various $CH_3NH_3PbI_3$ solar cells as a function of time when kept in (a) nitrogen, and (b) ambient environment.

**Figure S13.** Nyquist plot of impedance spectroscopy measured on various $CH_3NH_3PbI_3$ solar cells at 100 mW/cm$^2$ irradiation (bias = 0 V). Inset: equivalent circuit used to fit the impedance spectra.

**Table S1.** XPS peak percentage and ratio of corel level I 3d and Pb 4f of various $CH_3NH_3PbI_3$ films.

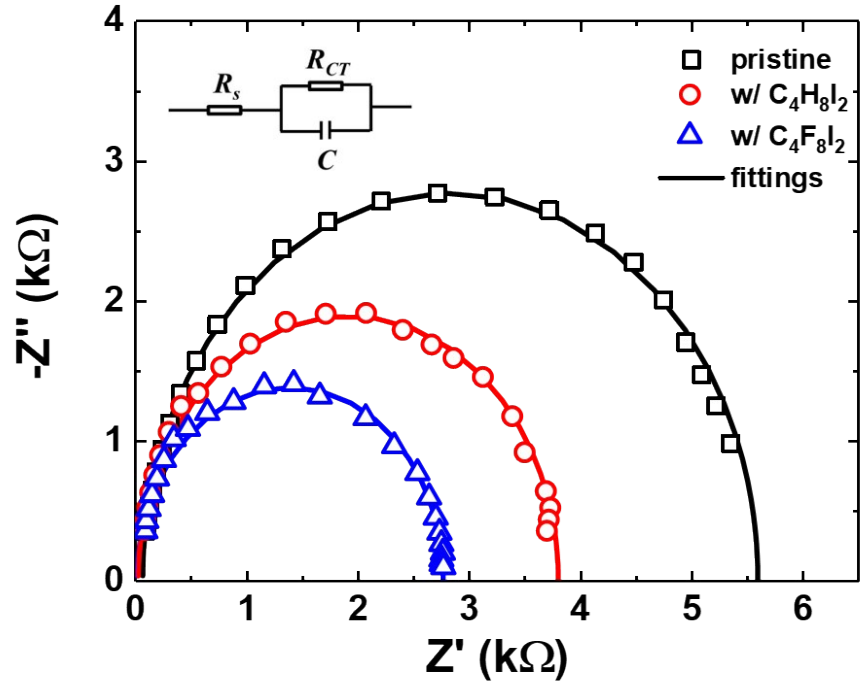| Element | pristine | w/ $C_4H_8I_2$ | w/ $C_4F_8I_2$ |
|---------|----------|----------------|----------------|
| I 3d | 38.795 % | 35.419 % | 46.737 % |
| Pb 4f | 14.737 % | 11.318 % | 15.812 % |
| I/Pb ratio | 2.63:1 | 3.13:1 | 2.95:1 |

**Table S2.** Time constants related to the fast ($\tau_1$) and slow ($\tau_2$) decays extracted from time-resolved PL spectroscopy of $CH_3NH_3PbI_3$ films.

| | $\tau_1$ (ns) | $\tau_2$ (ns) |
|---|---------------|---------------|
| pristine | 23.92 | 66.59 |
| $C_4H_8I_2$ (3%) | 25.46 | 68.74 |
| $C_4F_8I_2$ (3%) | 28.16 | 74.85 |

**Table S3.** $CH_3NH_3PbI_3$ solar cell parameters (best) processed with different concentrations of $C_4H_8I_2$ additives in the reverse scan direction.

| | $V_{oc}$ (V) | $J_{sc}$ (mA/cm$^2$) | FF (%) | PCE (%) |
|---|--------------|----------------------|--------|---------|
| 0 | 1.07 | 22.09 | 71.87 | 16.97 |
| 2.0% | 1.07 | 22.14 | 72.86 | 17.24 |
| 2.5% | 1.08 | 22.57 | 71.25 | 17.37 |
| 3.0% | 1.09 | 22.85 | 73.32 | 18.08 |
| 3.5% | 1.08 | 22.47 | 70.12 | 17.04 |

**Table S4.** $CH_3NH_3PbI_3$ solar cell parameters (best) processed with different concentrations of $C_4F_8I_2$ additives in the reverse scan direction.

| | $V_{oc}$ (V) | $J_{sc}$ (mA/cm²) | FF (%) | PCE (%) |
|---|---|---|---|---|
| 0 | 1.07 | 22.09 | 71.87 | 16.97 |
| 2.0% | 1.09 | 22.37 | 70.65 | 17.31 |
| 2.5% | 1.09 | 22.84 | 73.32 | 18.09 |
| 3.0% | 1.10 | 23.31 | 74.78 | 19.17 |
| 3.5% | 1.09 | 22.88 | 70.72 | 17.72 |

**Table S5.** $CH_3NH_3PbI_3$ solar cell parameters (best) processed with different concentrations of $C_6F_{12}I_2$ additives in the reverse scan direction.

| | $V_{oc}$ (V) | $J_{sc}$ (mA/cm²) | FF (%) | PCE (%) |
|---|---|---|---|---|
| 0 | 1.07 | 22.09 | 71.87 | 16.97 |
| 1.0% | 0.99 | 18.88 | 48.47 | 9.1 |
| 3.0% | 1.05 | 20.13 | 51.65 | 10.9 |
| 5.0% | 1.06 | 19.07 | 47.58 | 9.6 |
| 7.0% | 1.05 | 18.07 | 45.87 | 8.7 |

**Table S6.** $CH_3NH_3PbI_3$ solar cell parameters (best) processed with different concentrations of $C_8F_{16}I_2$ additives in the reverse scan direction.

| | $V_{oc}$ (V) | $J_{sc}$ (mA/cm$^2$) | FF (%) | PCE (%) |
|---|---|---|---|---|
| 0 | 1.07 | 22.09 | 71.87 | 16.97 |
| 1.0% | 1.06 | 19.46 | 71.83 | 14.92 |
| 3.0% | 1.04 | 18.18 | 66.16 | 12.46 |

**Table S7.** Device parameters of $CH_3NH_3PbI_3$ solar cell parameters extracted in the forward (F) and reverse (R) scan directions together with the calculated hysteresis index (HI).

| | $V_{oc}$ (V) | $J_{sc}$ (mA/cm$^2$) | FF (%) | PCE (%) | HI |
|---|---|---|---|---|---|
| control-F | 1.08 | 22.44 | 63.08 | 15.29 | |
| control-R | 1.08 | 22.45 | 71.95 | 17.46 | 0.224 |
| w/ $C_4H_8I_2$-F | 1.09 | 22.38 | 70.34 | 17.17 | |
| w/ $C_4H_8I_2$-R | 1.09 | 22.62 | 75.03 | 18.52 | 0.055 |
| w/ $C_4F_8I_2$-F | 1.09 | 23.21 | 73.07 | 18.49 | |
| w/ $C_4F_8I_2$-R | 1.09 | 23.57 | 78.18 | 20.12 | 0.050 |

**Table S8.** Parameters extracted from the the impedance spectrascopy measured on various $CH_3NH_3PbI_3$ solar cells under 100 mW/cm$^2$ irradiation (bias = 0 V).

| | pristine | w/ $C_4H_8I_2$ | w/ $C_4F_8I_2$ |
|---|---|---|---|
| $R_s$ ($\Omega$) | 63.53 | 29.57 | 18.35 |
| $R_{CT}$ ($\Omega$) | 5540 | 3782 | 2757 |
| $C_n$ (nF) | 5.26 | 5.45 | 5.47 |